Simulation of a muographic analysis of a volcanic dome in Geant4

Constantin D. Athanassas, C. Kitsaki, T. Alexopoulos, V. Gika, S. Maltezos

Simulation of a muographic analysis of a volcanic dome in Geant4

C.D. Athanassas, C. Kitsaki, T. Alexopoulos, V. Gika, S. Maltezos

Physics Department, National Technical University of Athens, Zografos, 15780, Athens, Greece

Abstract   *Here we present a Monte Carlo simulation of a muographic campaign on Methana volcano, Greece. In order to estimate the absorption parameters and the pattern of muon scattering at various incident energies (GeV to TeV), a radar-derived digital terrain model (DTM) was submitted to irradiation by horizontal muons in Geant4 and the penetrating muons were collected by a hypothetical MicroMegas particle detector on the other side of the DTM. Monte Carlo simulation demonstrated that muon energies at least as high as 10 TeV are required for whole-scale radiography of Methana and one has to reduce the scale of study to smaller structures (e.g. ~600 m - wide volcanic domes) in order to exploit the more affluent lower energy muons (~600 GeV). Coulomb scattering, on the other hand, brings about deflection of muon trajectories away from the detector, resulting in loss of information. Additionally, scattering adds Gaussian blurring to the scanned objects. With the intention of improving contrast and extract objects in muographic image we recommend the use of spatial operators (filters) employed in image analysis.*

Keywords   *muography, digital terrain model (DTM), detector; lava dome; Methana volcano*

INTRODUCTION

Geophysical exploration of the solid earth interior involves the introduction of some type of energy (i.e. electric, seismic or electromagnetic) and measurement in response to some physical property (i.e. electric resistivity, refraction or dielectric permittivity respectively). With the exemption of passive seismic tomography which utilizes the natural microseismicity [1] and gravimetry, radiography of volcanoes by cosmic rays is an alternative and inexpensive way that exploits the energy attenuation of cosmic muons crossing the volcano along different paths (Fig. 1) to gather information about its internal structure [2]. Cosmic-ray muon radiography (thenceforth termed *muography*) measures the cosmic ray flux deficit in the direction of observation and determines the integrated 2D density of a geological structure.

At near sea-level, cosmic rays primarily consist of relativistic muons with kinetic energies in the GeV– TeV range. Muons are charged particles (±) which arise from a series of decays of subatomic particles that are produced through spallation of atmospheric nuclei by colliding primary cosmic rays (i.e., higher-Z nuclei and protons) high up in the atmosphere. The differential flux of cosmic ray muons at the surface of the Earth is dependent on the polar angle theta (θ) but there is no expected dependence on the azimuth angle phi (φ).

In the Standard Model of particle physics [3], muons are the decay product of pions ($\pi^{\pm}$) and kaons ($K^{\pm}$):

$$\pi^{\pm} \rightarrow \mu^{\pm} + \bar{\nu}_{\mu}$$
$$K^{\pm} \rightarrow \mu^{\pm} + \bar{\nu}_{\mu}$$

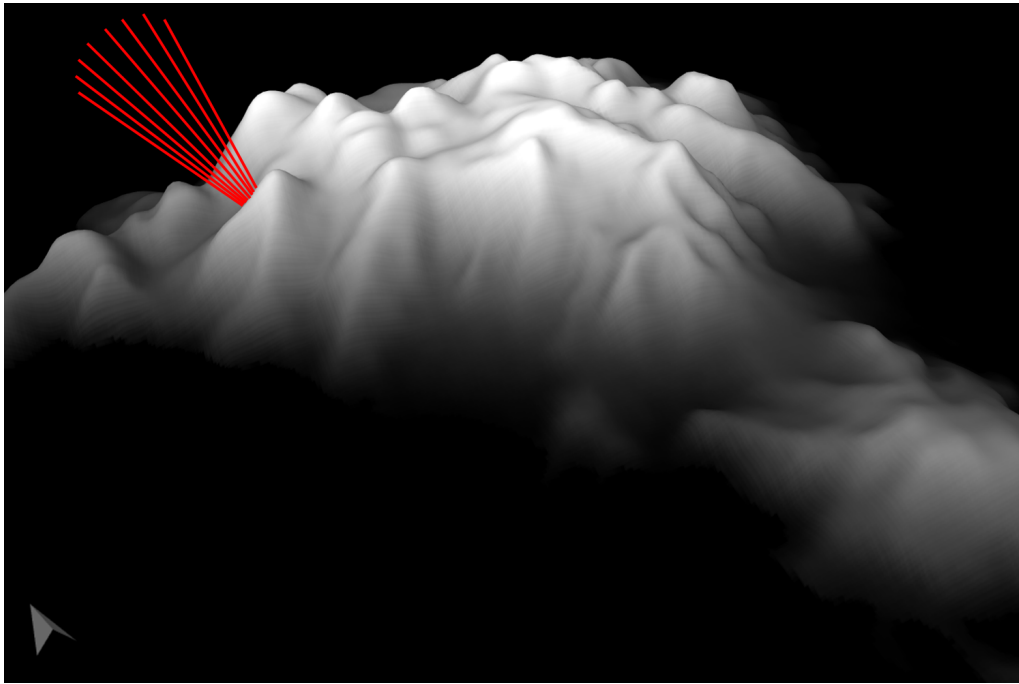and they themselves decay further to electrons, positrons and neutrinos:

C.D. Athanassas et al.

Figure 1. *Conceptual model of muography of a volcanic dome of Methana volcano.*

$$\mu^- \rightarrow e^- + \bar{\nu}_e + \nu_\mu$$
$$\mu^+ \rightarrow e^+ + \nu_e + \bar{\nu}_\mu$$

While traveling in the upper solid earth, muons interact with the atomic constituents of rocks and their energy attenuates (Eq. 1) through excitation and ionization of atoms (*ions*) and radiative processes, such as bremsstrahlung (*brem*), pair production (*pair*) and photonuclear reactions (*pn*).

$$\left(-\frac{dE}{dx}\right)_{tot} = \left(-\frac{dE}{dx}\right)_{ion} + \left(-\frac{dE}{dx}\right)_{brem} + \left(-\frac{dE}{dx}\right)_{pair} + \left(-\frac{dE}{dx}\right)_{pn} \qquad (1)$$

Muography employs particle detector technology and has been developed for imaging the integrity of nuclear reactors [4,5] and the internal structure of volcanoes [6-10]. Lately, muography is increasingly gaining ground in a greater number of geoscientific applications ranging from mining engineering to geotechnical engineering, the industry and more [2]. Density length X (hg·cm-2) is a key parameter of muography [6,8] which determines the amount of mass in the direction of observation. The higher the density and the longer the path (i.e. the larger the density length) cosmic muons travel in a volcanic edifice the lower their energy on exit. Muons that have intersected a volume of rock may reach the detector at a number (ν) given by the following expression [11]:

$$\nu(r_{m,n}, \Delta T) = I(r_{m,n}) \times \Delta t \times T(r_{m,n}) \qquad (2)$$

where, I (Eq. 3) represents the integrated muon flux crossing the geological edifice (cm^{-2}sr^{-1}s^{-1}) as a function of the incident differential flux Φ_0 (cm^{-2}sr^{-1}s^{-1}) and the minimum energy E_{min} (in GeV) necessary for muons to cross the edifice from edge to end for a given density length [11]:

$$I_{\varphi,\theta,X} = \int_{E_{min}}^{\infty} \Phi_0(E,\theta,\varphi)dE \tag{3}$$

Δt is the measurement duration (s) and T (cm²sr) is the acceptance of the detector, which is a measure of the its efficiency to collect a muon flux at a given solid angle, and depends on the geometrical characteristics of the detector (x,y dimensions, pixel size).

Various detector technologies (i.e. *muon telescopes*) have been employed in muography, ranging from nuclear emulsion plates to scintillators ([7,11]). Nuclear emulsion plate technology [12] provides high–resolution muographic images but their major drawback is that they only display the cumulative effect of the crossing muons. Gaseous tracking detectors [13] seem to be a true alternative to the presently popular scintillator-based detectors that reach the reliability of the latter and they can monitor density fluctuations in real time [14]. A promising technology is the MicroMegas detector (Micro–Mesh Gaseous Structure), which belongs to the genre of micro-pattern gaseous detectors (MPGD) with excellent time- and spatial resolution [15]. MicroMegas detectors are currently developed for the upgrade of the forward muon detectors of the ATLAS experiment at the Large Hadron Collider (LHC), CERN [16]. Recent efforts [17] in reducing the amount of electronics, consumption and cost can render these gaseous tracking stations practically deployable for muography.

Real-time observations have demonstrated that geological activity inside a volcano [18,19] is measurable by muography even before an eruption. This opens up a window for continual monitoring of active volcanoes not only for geoscientific purposes but also for hazard assessment and civil protection.

Insular volcanoes of the Aegean potentially pose major hazards to the region [20]. Methana volcano (Fig. 2) is a member of the active Hellenic volcanic arc, and it last erupted around 2.3 kyr ago [21]. It is a composite structure consisting of tens of volcanic domes [22]. Despite that fluid circulation is still ongoing on Methana, as seen from magnetotelluric and aeromagnetic data [23], the volcano has remained silent since the last eruption and for this reason it has been classified as dormant [24].

Nevertheless, the recent violent reawakening of the Sinabung volcano, Indonesia [25], which was previously classified as dormant too, justifies the need for close investigation and monitoring of volcanoes in Greece that have long been considered as dormant. Magnetotelluric prospection of Methana [26] mainly probes several kilometers beneath the volcano, but little is known as to the spatial distribution of near-surface geological structures (conduits) that could well-up magma in a future eruption. Muography has the potential to explore and monitor Greek volcanoes on a real-time basis, being decisive in providing early warnings of volcano reawakening.

In the absence of a theoretical model of cosmic-ray propagation through a volcano, experimental data would only have a qualitative character. Quantification can thus be achieved only through simulations that allow comparison between theoretical estimates and experimental data. As the nature of muon propagation through matter does not allow for analytical solutions *Monte Carlo* simulation is typically employed to conceive a model of the muon-rock interactions [27]. This work estimates through Monte Carlo simulation the contribution of various processes to muon attenuation (radiative and ionizing) for a volcanic dome of Methana, as well as evaluates quantities such as range and Coulomb scattering angles on a hypothetical MicroMegas detector placed in front of the dome. Finally, it delivers a model of density length for the said volcanic dome derived from topographic data.
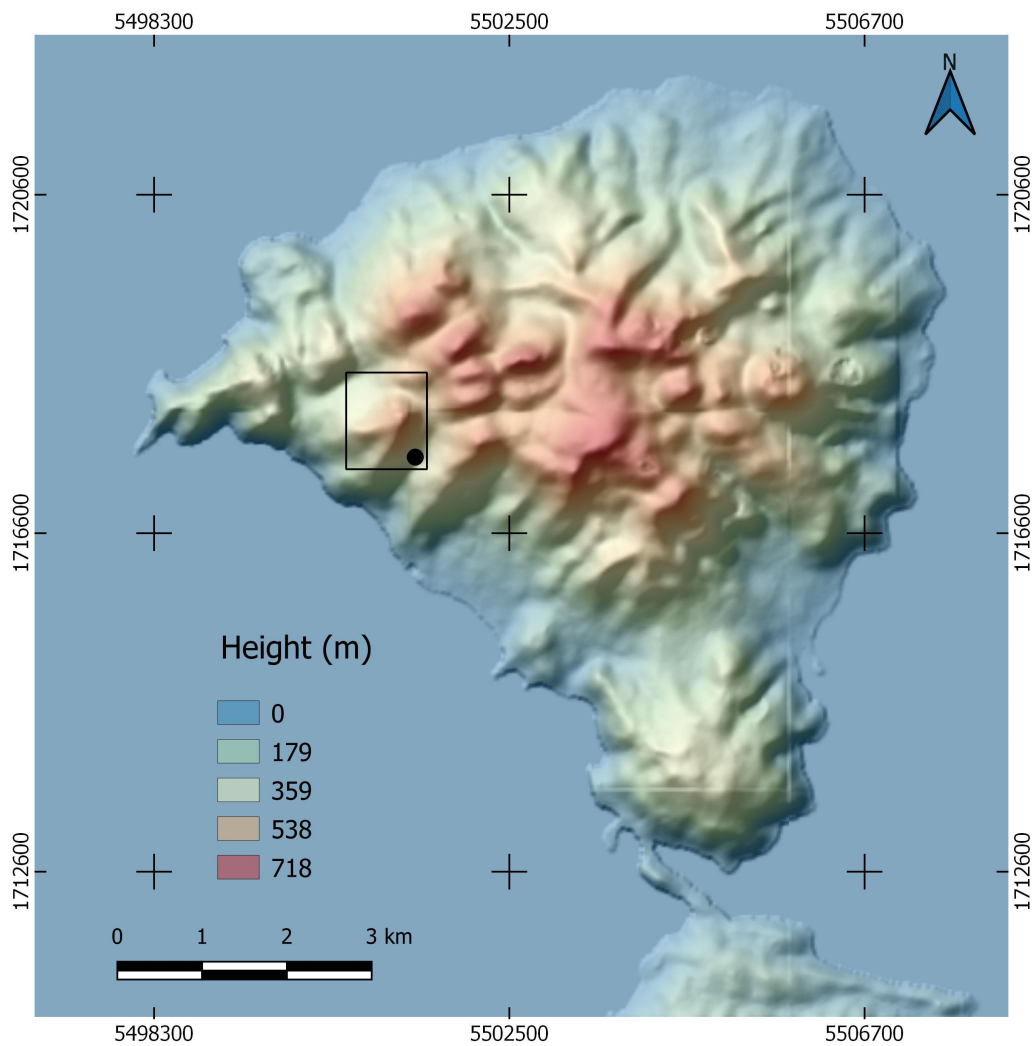
Figure 2. *Digital terrain model of the Methana volcano. Source data: EU-DEM - a hybrid 3D raster DTM (GeoTIFF) combining SRTM (Shuttle Radar Topography Mission) and ASTER (Advanced Spaceborne Thermal Emission and Reflection Radiometer). Coordinate reference system EPSG:3035 - ETRS89 / LAEA Europe – Projected. The grid-like lines on the right of the map is an artifact of EU-DEM's image processing. Black dot represents the detector position whereas the rectangle envelopes the scanned volcanic dome.*

MODEL SETUP AND SOURCE DATA

Simulation was carried out in Geant4 [28] because the latter is efficient in handling complex geometries and includes detailed multiple–Coulomb scattering models. In order to reduce the computational time we submitted to irradiation only a small excerpt of the entire DTM (framed by the rectangular in Fig. 2) which corresponds to a ~600 m × 600 m volcanic dome (Fig. 2), in the vicinity of the volcanic center erupted 2.3 kyr ago.

The DTM used here is the EU-DEM, which is a hybrid 3D raster DTM (GeoTIFF) combining SRTM (Shuttle Radar Topography Mission) and ASTER (Advanced Spaceborne Thermal Emission and Reflection Radiometer) data (Fig. 2) with spatial resolution (i.e. pixel size) of 25 m. In a computational region of Geant4 a virtual adaptation of the specific volcanic dome of Methana (Fig. 3)

was constructed by paving the digital terrain model (DTM) with voxels ('3D pixels') identified with physical volumes of vertical cuboids appended with SiO_2 material (density 2.6 g·cm^{-3}) and cross-section and height dimensions determined by the pixel attributes of the DTM.

The computational region outside the DTM in Geant4 was filled with air (1 atm). A virtual detector designed as a matrix consisting of cells (pixels) filled with argon, each of them defined as 'sensitive' was added to the model to represent a single 5–mm thick MicroMegas panel. Two different granularities (pixel sizes) were considered for testing: 1m × 1m and 0.5 m × 0.5 m, respectively.
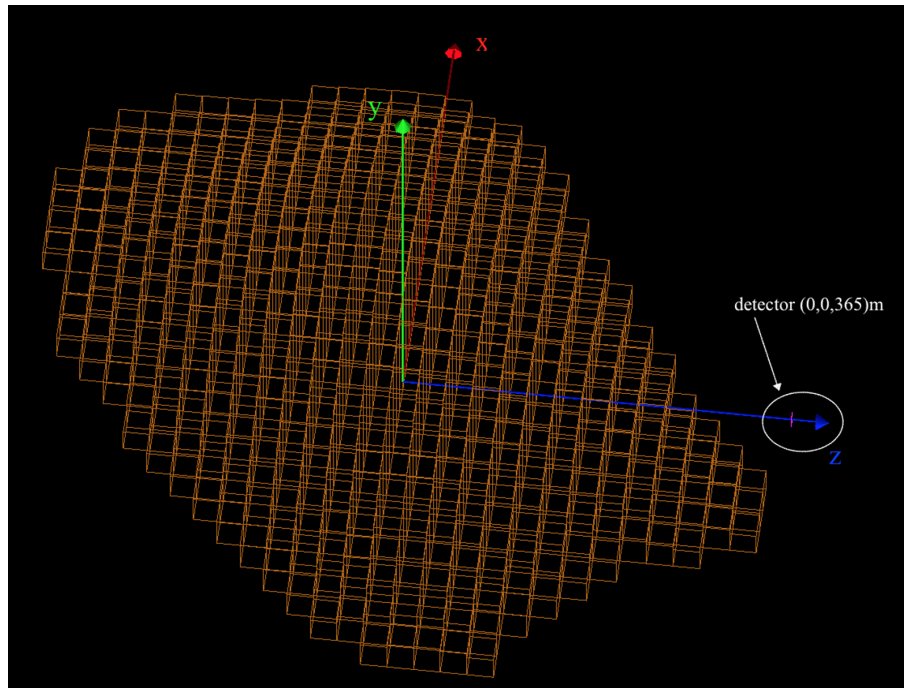

Figure 3. Model of the volcanic dome of the Methana volcano consisted of parallelepiped physical volumes (voxels) in the Geant4 computational region. X-axis (up) points East. The detector is placed south of the dome.

Incident muon flux is not only a function of altitude and the polar angle but also of the muon energy. Analytical approximations lack the wanted precision and a Monte Carlo approach is usually preferred [29,30]. However, it has been found that muons with nearly horizontal trajectories can penetrate deeper in solid rock, as deep as ~1 km approximately [31,32] and for this reason they are preferred for muography of large salient geological structures over those coming from showers from all directions [7], despite their lower intensity (and the, thus, longer exposure times required). Here, rays of horizontal muons were used (Fig. 4) to calculate range and scattering angles. The modeled volcanic dome was exposed to μ-beams of increasing energy stepwise (in the GeV range) and its response as to the interaction parameters was measured.

RESULTS AND DISCUSSION

The results of the simulation experiments, performed in Geant4, are summarized in the following graphs, which were generated using ROOT software. Fig. 5 illustrates the energy loss per unit length at various muon energies. Bremsstrahlung and pair production (radiative) processes overtake ionization in the energy loss for the given rock type and density at ejection energies ≥300

GeV and grow at a rate nearly proportional to the energy. This point, which is defined as the energy at which the two loss rates are equal, is known as critical energy. Critical energy is twice as small as the value calculated for standard rock in the literature [33,34].
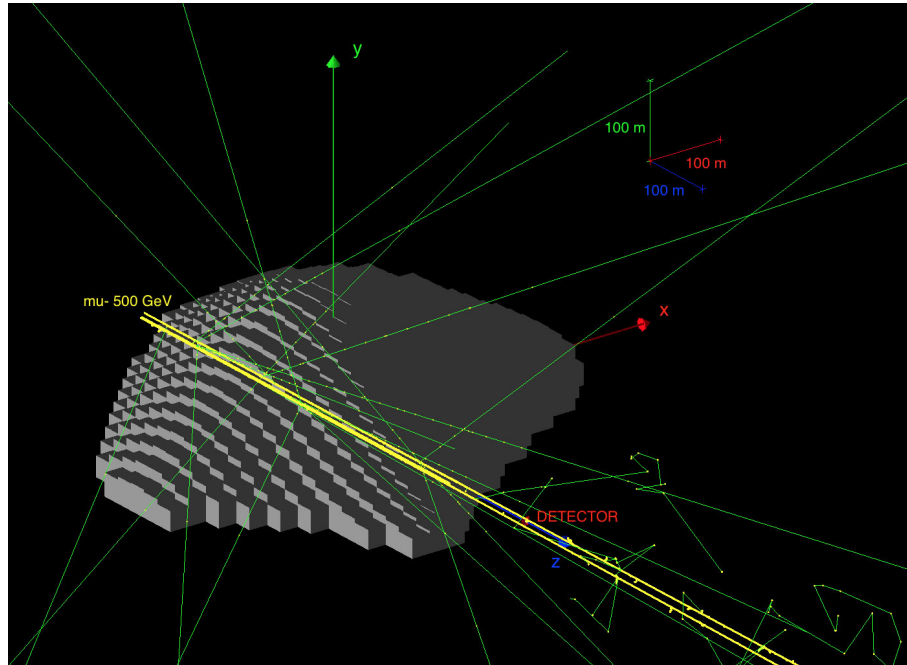

Figure 4. Schematic illustration of the simulation framework of the volcanic dome of Methana in Geant4. Yellow lines correspond to muon trajectories while jagged green lines represent photon tracks due to Compton scattering. X axis points East.
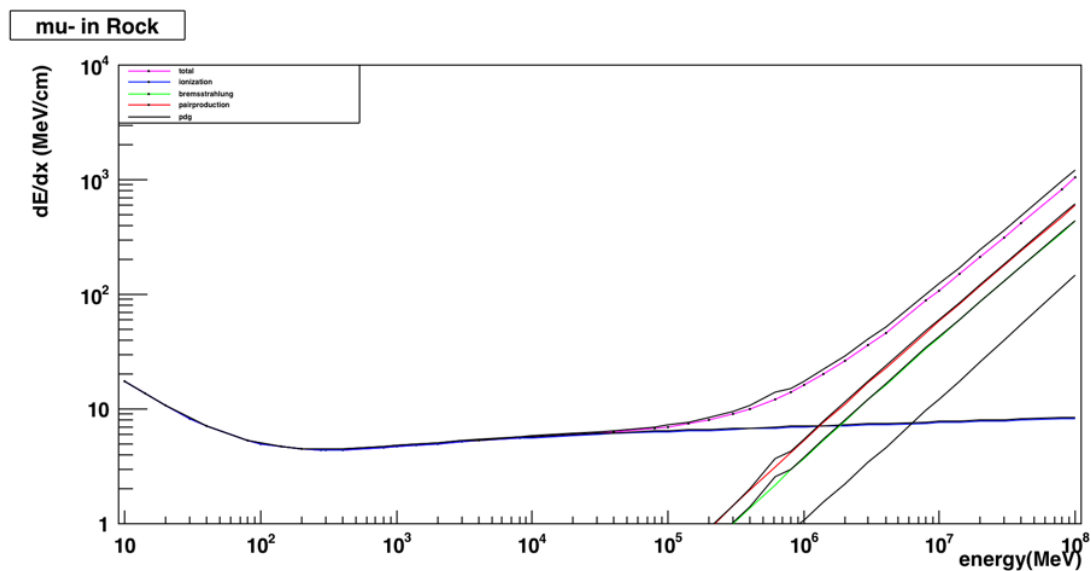

Figure 5. *Contributions of various processes (radiative and ionizing) to the muon energy loss as a function of the injection energy (MeV)*

The next parameter evaluated was the penetration depth (range). Fig. 6 demonstrates (with the blue line) the range of the muon beam (in cm) as a function of the injection energy up to 10^4 GeV (10 TeV) and contrasts it against the continuous slow down approximation (CSDA; with the brown line) range (Eq. 4; [35]),

$$R(E_0) = -\int_0^{E_0} \frac{dE}{dE/dx} \tag{4}$$

where E_0 corresponds to the injection energy. They seem to be in good agreement with each other. It, thus, follows that energies at least 10 TeV are required in order the entire volcano to be fully penetrated by muons, while the smaller structure studied here (i.e. volcanic dome) can be fully penetrated by ~ 600 GeV muons.

With regard to scattering, the deviation that muons experience while transversing the medium along both polar and azimuth angles was estimated by shooting multiple particles from a point source opposite the dome in the direction of the detector at elevating energies. Fig. 7 summarizes the scattering information for each injection energy showing, as expected, that the higher the energy the tighter the distribution of the scattering angles.

Fig. 8 and Fig. 9 illustrate the spatial (2D) distribution of muon scattering on the detector surface. The matrix represents a simulated MicroMegas detector against which muons are sequentially shot from a point source opposite the volcano (for the 900 GeV muons). Since a virtual environment like Geant4 does not pose any design restrictions the effective area was enlarged for wider observation of particle scattering using different detector granulatries. It is obvious that Coulomb scattering incurs Gaussian blurring on the scanned objects, turning point objects into rough circles.
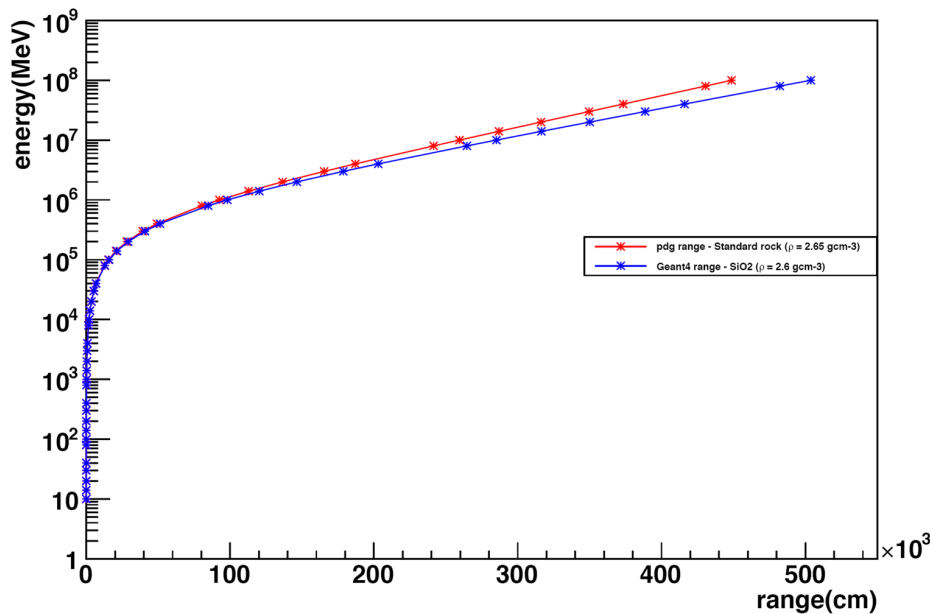

Figure 6. The range as a function of muon injection energy (blue) in comparison with the CSDA approximation (brown).

Finally, a model of the theoretical density length was calculated (Fig. 10). The length of variable trajectories converging to a (0,0) were multiplied by the supposed average density of the lava dome. Any deviation between the modeled density length shown in Fig. 9 and the observed density length

(from the telescope; forthcoming measurements) would imply density discontinuities which can be translated as structural discontinuities inside the geological edifice.
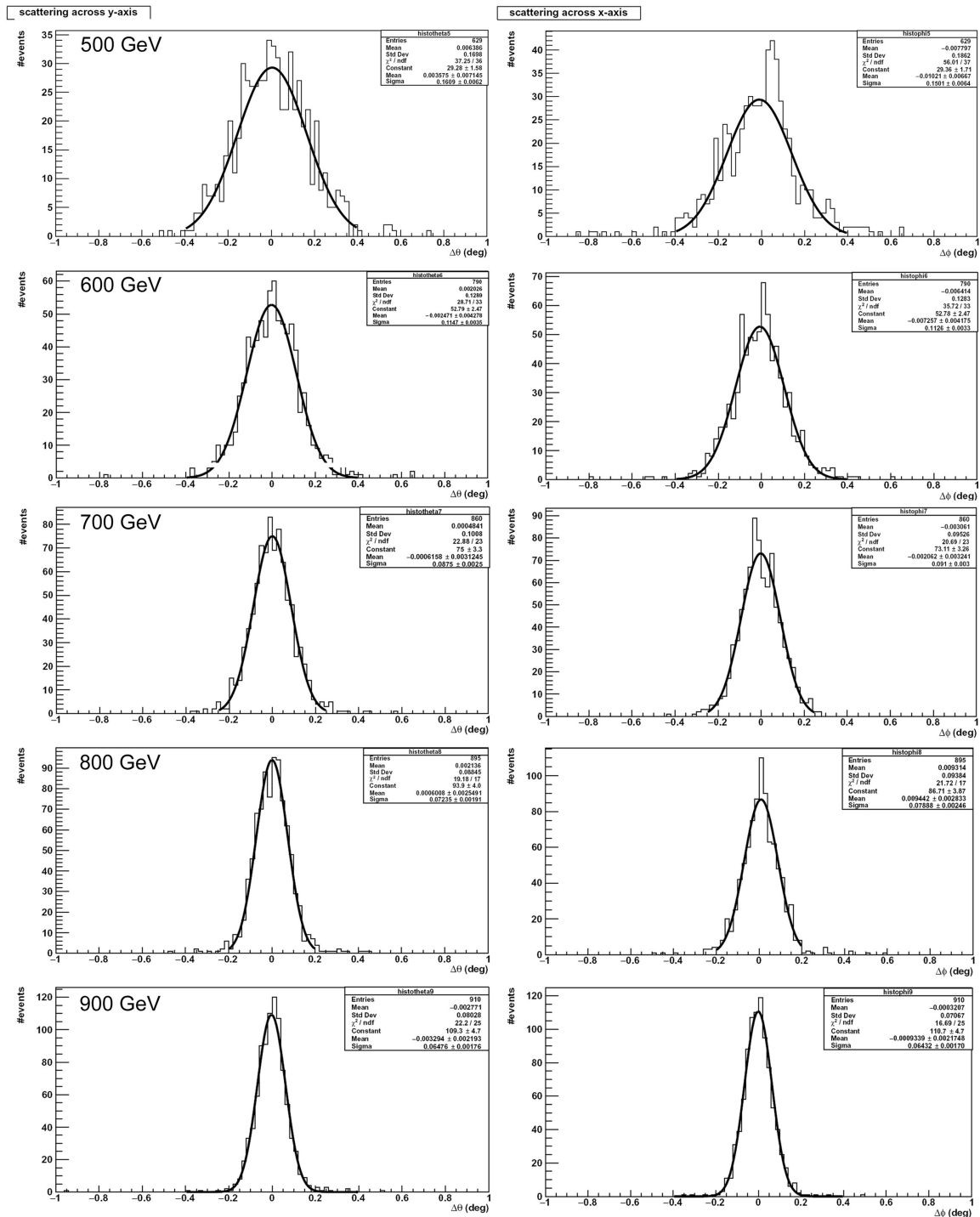

Figure 7. Distribution of muon scattering angles at elevated injection energies for X- and Y-axis
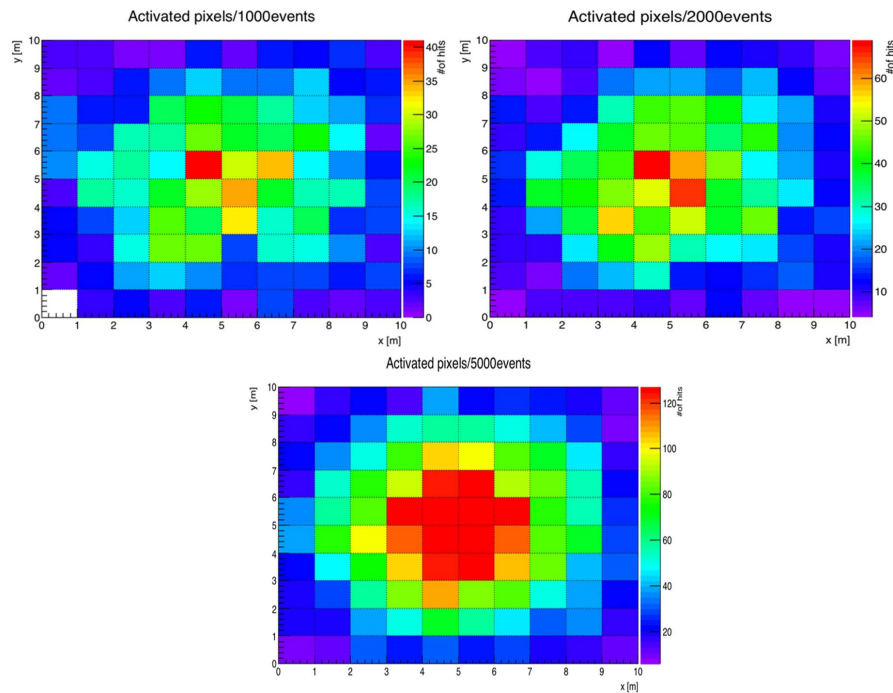
Figure 8. Count distribution on the MicroMegas detector of 1000 (top left), 2000 (top right) and 5000 (bottom) muons injected at 900 GeV. Resolution set to 1×1 m. (y,x axes in meters; number of muon hits represented as colors)
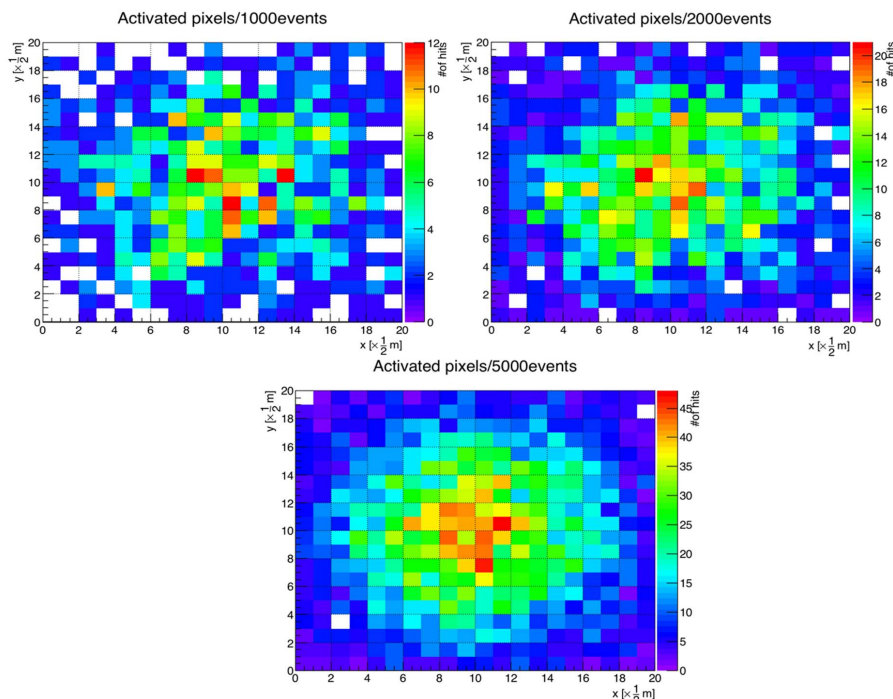

Figure 9. Count distribution on the MicroMegas detector of 1000 (top left), 2000 (top right) and 5000 (bottom) muons injected at 900 GeV. Resolution set to 0.5×0.5 m. (y,x axes in meters; number of muon hits represented as colors)
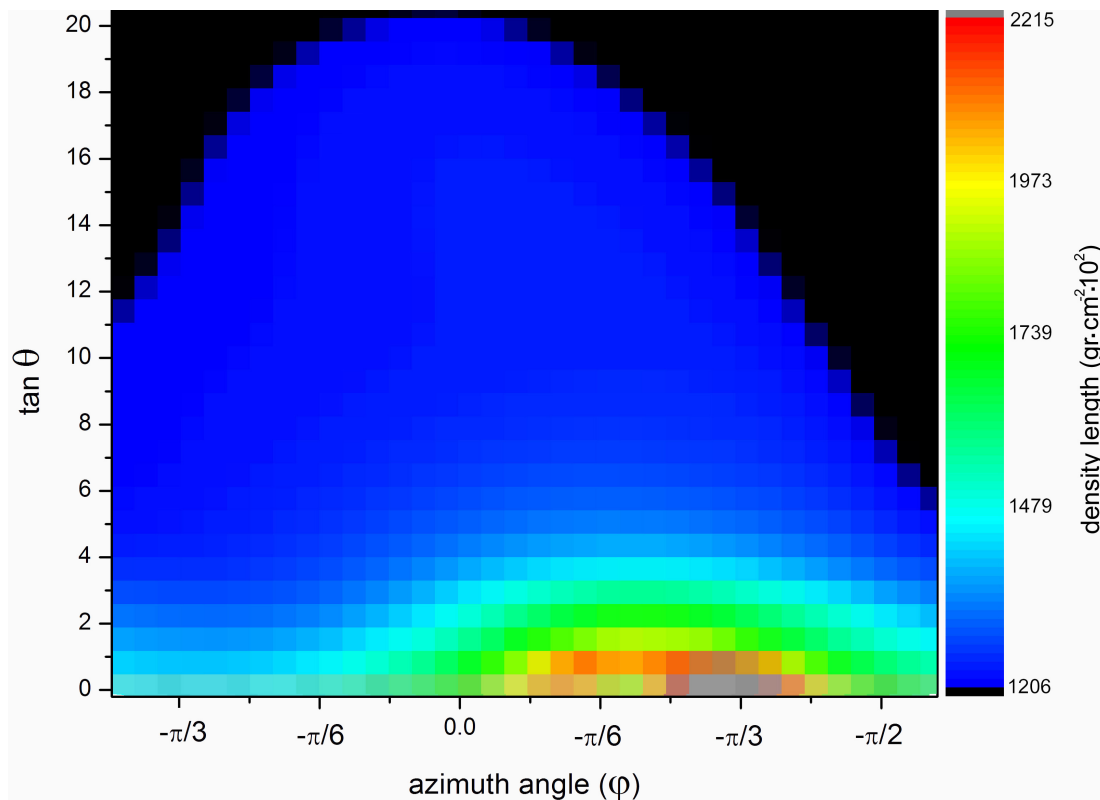
Figure 10. Density length model of the volcanic dome of Methana concerned here. Color-graded scale on the right provides the density length estimates (gr·cm^{-2}·10^{-3}) in the (φ,θ) direction.

CONCLUSIONS

Here, we simulated a muographic campaign of a volcanic dome of Methana volcano in Geant4, by exposing an open access radar–derived DTM to horizontal muon beams of various energies. Calculations of the range showed that muon beams should be energetic enough, at least 10 TeV, in order to fully penetrate the entire volcano. At those energies muon attenuation is controlled by radiative processes also. However, events in the TeV range are scarce [36] and impractical for muography. It is thus recommended that the area under surveillance be gridded in smaller segments of the size of the dome studied here so that the more affluent lower energy muons (~600 GeV) can be exploited swiftly and ensure timely muographic images.

Coulomb muon scattering has the unwanted but unavoidable effect of blurring the image such that point objects appear as disks with soft edges. Although higher–energy muons will return less blurred images (since they undergo less deflection while traveling through the medium) blurring cannot be fully prevented. This situation is analogous to Gaussian blurring in conventional photography, where images suffer from some degree of degradation because of the image formation process or external factors such as atmospheric distortions etc. We promote the convolution of spatial filters employed in signal (image) analysis such as the Tikhonov regularization or the conjugated methods. These are inverse-problem solving methods that aim at reconstructing a Gaussian-blurred image. These aforesaid theoretical results will drive the forthcoming experimental study on Methana.

Acknowledgments

References

[1]   G.A. Tselentis et al., Geophysics 73, 89 (2013), doi: 10.1190/1.3560016
[2]   S. Procureur, Nucl. Inst Meth. Phys. Res. A 878, 169 (2018), doi: 10.1016/j.nima.2017.08.004
[3]   T.K. Gaiser et al. Cambridge University Press, 444p (2016), doi: 10.1017/CBO9781139192194
[4]   K. Borozdin et al., Phys. Rev. Lett. 109, 152501 (2012)
[5]   Perry et al., J. App. Phys. 113, 184909 (2013), doi: 10.1063/1.4804660
[6]   H.K.M. Tanaka et al., Geoph. Res. Lett. 34, L22311 (2007), doi: 10.1029/2007GL031389
[7]   H.K.M. Tanaka et al., Nucl. Inst Meth. Phys. Res. A 555, p.164 (2005),
      doi: 10.1016/j.nima.2005.08.099
[8]   H.K.M. Tanaka et al., Nucl. Inst Meth. Phys. Res. A 575, p. 489 (2007),
      doi: 10.1016/j.nima.2007.02.104
[9]   N. Lesparre et al., Geoph. J. Int. 183, 1348 (2010), doi: 10.1111/j.1365-246X.2010.04790.x
[10] C. Cârloganu et al., Geosci. Instrum. Method. Data Syst. 2, 55 (2013), doi: 10.5194/gi-2-55-2013, 2013
[11] N. Lesparre et al., Geophys. J. Int. 185, 1 (2012), doi: 10.1111/j.1365-246X.2012.05546.x
[12] K. Morishima, Phys. Proc. 80, 19 (2015), doi: j.phpro.2015.11.082, doi: 10.1016/j.phpro.2015.11.082
[13] L. Oláh et al., Sci. Rep. 8, 3207 (2018), doi: 10.1038/s41598-018-21423-9
[14] D. Varga et al., Adv. High Energy Phys, 1962317 (2016), doi: 10.1155/2016/1962317
[15] T. Alexopoulos et al., J. Inst. 5, P02003 (2010), doi: 10.1088/1748-0221/5/02/P02003
[16] T. Alexopoulos et al., Nucl. Inst Meth. Phys. Res. A 617, p.11 (2010), doi: j.nima.2009.06.113
[17] S. Bouteille et al., Nucl. Inst Meth. Phys. Res. A 834, 223 (2016), doi: 10.1016/j.nima.2016.08.002
[18] H.K.M. Tanaka et al., Geoph. Res. Lett. 36, L17302 (2009), doi: 10.1029/2009GL039448
[19] K. Joudre et al., Sci. Rep. 6, 33406 (2016), doi: 10.1038/srep33406
[20] G. Vougioukalakis & G. Fytikas, Develop. Volc. 7, 161 (2005), doi: 10.1016/S1871-644X(05)80037-3
[21] G. Pe-Piper & D.J.W. Piper, J. Volc. Geoth. Res. 260, 146 (2013),
      doi: 10.1016/j.jvolgeores.2013.05.011
[22] V. Dietrich & P. Gaitanakis. Geol. map of Methana. ETH Zurich, Switzerland (1995)
[23] A. Efstratiou et al., Geoph. Res. Abstr., 14, EGU2012-11673-1 (2012)
[24] W. D'Alessandro et al., J. Volc. Geoth. Res. 178, 818 (2008), doi: 10.1016/j.jvolgeores.2008.09.014
[25] H. Gunawan et al., J. Volc. Geoth. Res. 382, 103 (2017), doi: 10.1016/j.jvolgeores.2017.08.005
[26] T.K. Volti, Tectonophysics 301, 111 (1996), doi: 10.1016/S0040-1951(98)00218-2
[27] R. Nishiyama et al., Geoph. J. Int. 206, 1039 (2016), doi: 10.1002/2013JB010234
[28] S. Agostinelli et al., Nucl. Instr. Meth. A 506, 250 (2003), doi: 10.1016/S0168-9002(03)01368-8
[29] S. Béné et al., Geosci. Instrum. Method. Data Syst. 2, 11 (2013), doi: 10.5194/gi-2-11-2013
[30] R. Nishiyama et al., Geoph. J. Int. 206, 1039 (2016), doi: 10.1093/gji/ggw191
[31] K. Nagamine et al., Nucl. Instr. Meth. A 356, 585 (1995), doi: 10.1016/0168-9002(94)01169-9
[32] K. Nagamine et al., Geoph. Res. Abstr. EGU05-A-10764 (2005)
[33] K. Nakamura et al., J. Phys. G 37, 075021 (2010), doi: 10.1088/0954-3899/37/7A/075021
[34] A. Lechman et al., Solid Earth, 9, p.1517 (2018), doi: 10.5194/se-9-1517-2018
[35] N.J. Carron, Taylor and Francis, 384p. (2007)
[36] Pierre Auger Observatory, auger.org. (Retrieved 20 August 2018).